Int. J. Electrochem. Sci., 11 **(2016)** 9666 – 9675, doi: 10.20964/2016.11.28

International Journal of
ELECTROCHEMICAL
SCIENCE
www.electrochemsci.org

Influence of Multi-Pass Welding on the Microstructure Evolution and Corrosion Resistance of a Super Duplex Stainless Steel

Yangting Sun, Xiayu Wu, Xuan Wu, Jin Li, Yiming Jiang[*]

Department of Materials Science, Fudan University, Shanghai 200433, China
[*]E-mail: corrosion@fudan.edu.cn

Received: 8 August 2016 / *Accepted:* 5 September 2016 / *Published:* 10 October 2016

Different thermal simulations of multi-pass welding were performed on the 2507 duplex stainless steel. The influence of thermal cycles on microstructure and phase ratio was studied. The toughness and pitting resistance of different specimens were investigated through impact energy test and critical pitting temperature test, respectively. The results revealed that the microstructure and performance of 2507 were deteriorated significantly after single-pass welding. While welding pass increased, the restoration effect was observed.

Keywords: Duplex stainless steel; Multi-pass welding; Heat-affected zone; corrosion

1. INTRODUCTION

Duplex stainless steels (DSS), characterized by the two-phase microstructure of austenite (γ) and ferrite (α), are widely used in corrosive environments because of the combination of excellent mechanical strength and corrosion resistance. Their great performance largely depends on the balanced phase ratio, which consists of approximately equivalent amount of α and γ without detrimental precipitates [1-3]. However, the welding process, which is indispensable during practical use, will result in microstructure evolution in DSSs and then degrade their mechanical properties and corrosion resistance [3-10]. Besides, the precipitation of deleterious secondary phase such as carbides, nitrides, secondary austenite, sigma (σ) and chi (χ) will also impair the DSSs' performance [11-14]. During the practical welding, the weld metal zone (WMZ) undergoes a fusion process whereas the heat-affected zone (HAZ) experiences a heat-cooling process. Because the higher-alloyed materials are used as solder under gas protection, the mechanical properties and corrosion resistance of WMZ tends to be

better than those of HAZ [8, 9]. Therefore, large numbers of investigations has focused on the HAZ of DSSs [5, 15-20].

In practical use, multi-pass welding is adopted to replace single-pass welding for it can restore the unbalanced microstructure. Our previous work has demonstrated this phenomenon on DSS2304 [21]. The influence of cooling rate and Cr_{eq}/Ni_{eq} value on microstructure and corrosion resistance has also been investigated [22, 23]. In this paper, we focus on 2507, another DSS which is higher alloyed than 2304, for the effect of multi-pass welding on mechanical and corrosive properties of 2507 is still scarce.

The thermal simulations from first pass to third pass were performed through Gleebe thermal-mechanical simulator. Subsequently, the microstructure was observed by optical microscope and the pitting resistance was characterized by CPT (Critical Pitting Temperature) method. In addition, the similarities and differences between 2304 and 2507 were also discussed.

2. EXPERIMENTAL

2.1. Material

The material studied in this work was super duplex stainless steel (SDSS) 2507 that was manufactured by Baosteel. The chemical composition was listed in Table 1 and the composition of 2304 used for comparison was also provided.

Table 1. Chemical composition of DSS 2507(wt.%)

Elements	Cr	Ni	Mo	N	Mn	C	Si	S	P	Cu
2507	25.15	6.74	3.43	0.27	0.69	0.022	0.55	0.002	0.029	0.13
2304	23.23	4.8	0.42	0.12	1.49	0.016	0.38	0.001	0.025	0.3

The samples were melted in a 50 kg vacuum furnace and then cast into single square ingots. After removing the oxide skin, the ingots were forged into square blooms at the temperature ranging from 900 to 1200 °C and divided into several blooms with a dimension of 150 mm × 100 mm × 42 mm. The blooms were reheated at 1250 °C for 2 h and hot-rolled, using a laboratory hot-rolling mill, into 12mm thick plates. Before thermal simulation, these plates were subjected to a solution treatment at 1080 °C for 12 min and then quenched in water. At last, the solution-annealed plates were cut into the dimensions of 10 mm × 10 mm × 55 mm with the longitudinal direction paralleling to the rolling direction.

2.2. Thermal simulation

To investigate welding process, thermal simulation was an effective and widely applied method which was performed in a thermos-mechanical simulator [11, 16-18]. As was shown in Fig. 1 and

described in our previous work [21], different locations in the HAZ experienced different thermal cycles during practical multi-pass welding.

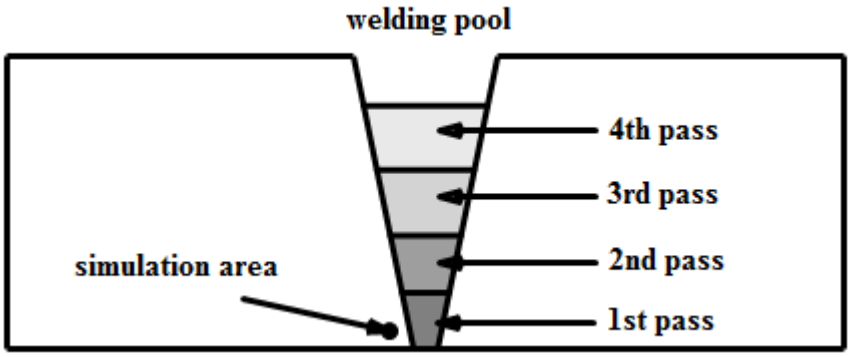

Figure 1. Sketch of joints in multi-pass welding. The cycle at the joint bottom referred to the point for thermal simulation.

In current work, we concentrated on the high temperature HAZ which was near the bottom area of weld pool. The simulation process was performed by Gleebe 3800 thermal-mechanical simulator and the thermal cycle was established according to Rosenthal's solution of heat transfer equation [24]. The peak temperature in the first-pass welding thermal cycle arrived at 1350 °C and the cooling rate between 1350 °C and 800 °C was about 30 °C/s; The second peak temperature was 1050°C and the corresponding cooling rate to 400 °C was about 3 °C/s; The peak temperature in the third-pass welding was 700 °C and the cooling rate between 700 °C and 400 °C was about 2 °C/s. Only three cycles were carried out because the fourth pass welding with a peak temperature lower than 400°C had little influence on the duplex stainless steel. The specimens were respectively named as single-pass HAZ, double-pass HAZ and triple-pass HAZ after different thermal cycles.

2.3. Electrochemical testing

The critical pitting temperature measurement (CPT) was a rapid method to evaluate the pitting corrosion resistance of DSSs. Compared with the more-often used pitting potential, it was more sensitive and easier to be reproduced [25].

In this paper, CPT measurements were carried out in 1.0M NaCl deaerated solution using the potentiostat PARSTAT MC (PMC) 500 with a three-electrode cell. A platinum foil and a saturated calomel electrode (SCE) worked as the counter electrode and reference electrode respectively. The specimens acting as the working electrode were cut from the thermal simulated specimen into the dimension of 10 mm × 10 mm × 4 mm and then embedded in epoxy resin with a 1 cm^2 exposure area, which made the traverse plane to be the testing surface. Before the CPT test, each specimen was abraded mechanically with a series of abrasive papers from 180 to 2000 grit and then polished with 1.5 μm diamond paste. Special process was adopted to avoid crevice corrosion [26]. During the test, the specimen was firstly cathodic polarized at -900 mV (SCE) for 2 min. This process could deoxidize the

surface of working electrode and improve the reproduction of the test [27]. Then the open circuit potential was carried out at room temperature for 20 min to stabilize the surface of the working electrode. At last, an anodic potential of 700 mV (SCE) was applied on the specimen and the solution temperature was increased at a rate of 1 ± 0.3 °C/min from 35 °C, according to ASTM G150. The temperature was detected through a Pt-100 RTD. Simultaneously, the current density was recorded until it reached about 400 μA/cm^2. The CPT was defined as the temperature where the current density equaled to 100 μA/cm^2. Throughout the test, pure nitrogen gas was bubbled into the solution to exclude the influence of oxygen gas. To guarantee the accuracy of the results, the measurement of each specimen was repeated for 3 times and the final value of CPT was the average data.

2.4. Microstructure analysis

The optical metallurgical microscope (OM 4XG) was used to observe the two-phase microstructure of the duplex stainless steels. Prior to the observation, the specimens were etched by 30% KOH electrolyte at 2 V (SCE) for 15 s. The volume fraction of ferrite and austenite were evaluated by computer aided quantitative metallography. Over 10 measurements were carried out to obtain the ultimate average value. Morphologies of the pits after CPT tests were observed by scanning electron microscopy (SEM Philips XL 30 FEG).

3. RESULTS AND DISCUSSION

3.1. Microstructure evolution

The equilibrium diagram of DSS 2507 was described in Fig. 2 by the Thermo-Calc software. As shown in the diagram, the phase-balance temperature (T_b) at which ferrite phase and austenite phase had equal fraction was 1096 °C. This was why the solution treatment temperature was set at 1080 °C, near the T_b. When the 2507 experienced thermal process above the T_b, the austenite phase tended to transform into ferrite phase. This phenomenon is known as ferritization.

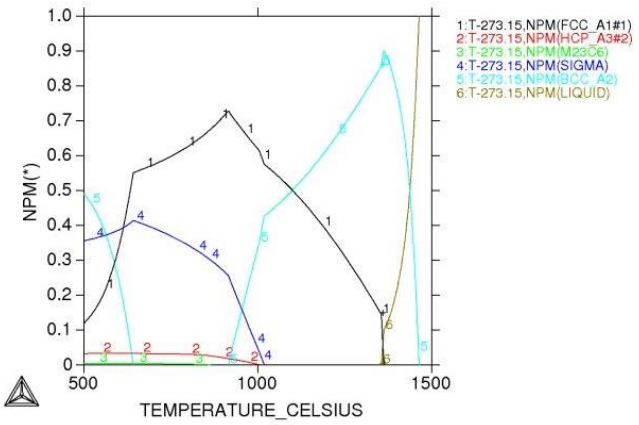

Figure 2. Equilibrium diagram of DSS 2507 calculated by Thermo-Calc software. 1.austenite, 2.chromium nitride, 3.$M_{23}C_6$, 4.sigma, 5.ferrite, 6.liquid.

Fig. 3 presented the optical microstructures of DSS 2507 base metal and thermal simulated specimens. It was displayed that white γ-islands were embedded in the gray etched δ-ferrite matrix. Ferrite phase fraction in the base metal was 49.6% as shown in table 2. After the first pass thermal cycle, the original phase ratio was destroyed and the ferrite fraction increased to54.7% due to the ferritization. In our previous work, this effect was more severe in DSS 2304, viz. 2507 reserved relatively more original-austenite during the same thermal simulation to first-pass welding [21]. This was because the contents of Ni and N in 2507 were largely higher than those in 2304. As the former and stabilizer elements of austenite, they could notably prevent the transformation from austenite to ferrite. Unlike 2304, in the equilibrium diagram of 2507, see Fig. 2, there was no ferritized temperature (T_f) in the strict sense. In the high temperature about 1360°C, austenite phase had not totally transformed into ferrite, while the liquefaction was observed.

Table 2. Phase ratio of DSS 2507 after different thermal simulation.

Specimen	BM	Single-pass	Double-pass	Triple-pass
Ferrite fraction (%)	49.5	54.7	52.0	51.8

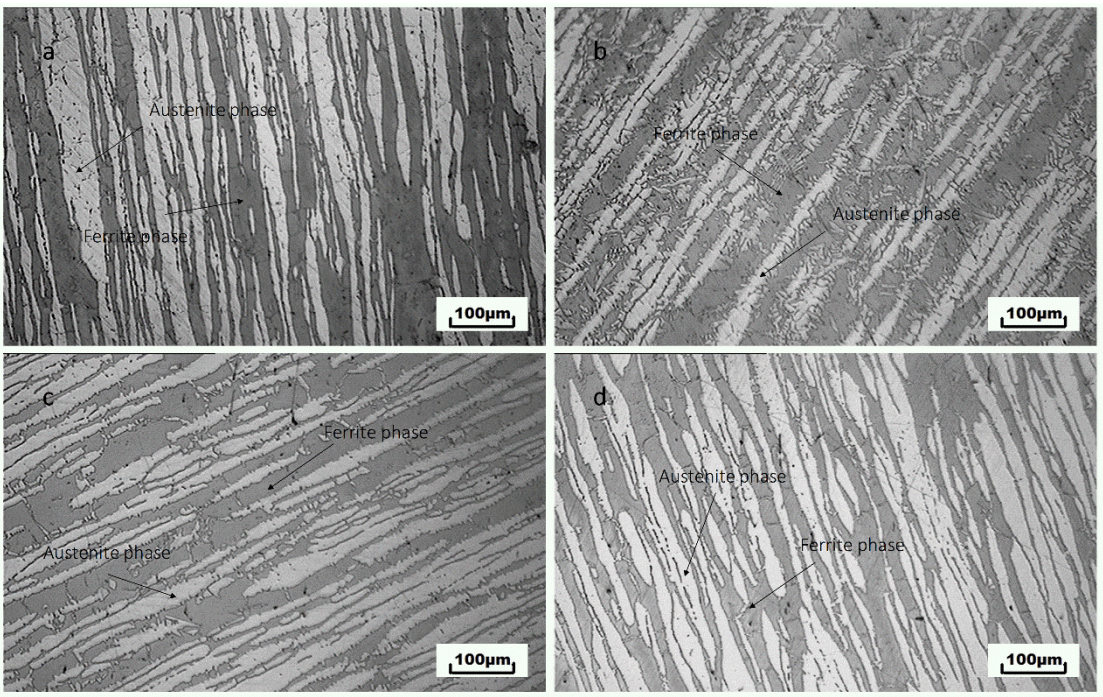

Figure 3. Microstructure of DSS 2507 base metal and HAZ specimens after different thermal cycle. Electrolyte: 30% KOH; applied potential: 3V; etching time: 15s. a. base metal; b. single-pass HAZ; c. double-pass HAZ; d. triple-pass HAZ.

As was shown in Fig. 3c and d, the amount of ferrite in HAZ after second and third pass thermal cycle slightly decreased with some tiny austenite appearing in ferrite grains or along the phase boundaries. This phenomenon was more obvious in second-pass HAZ, which demonstrated that the

unbalanced phase ratio resulted from the first-pass could be fixed by the second-pass welding thermal cycle. It was similar to a simple solid solution treatment, which could amend the microstructure of DSSs and improve their properties [28, 29]. Compared with 2507, the restoration of lower-alloyed 2304 was more obvious [21].

3.2. Toughness

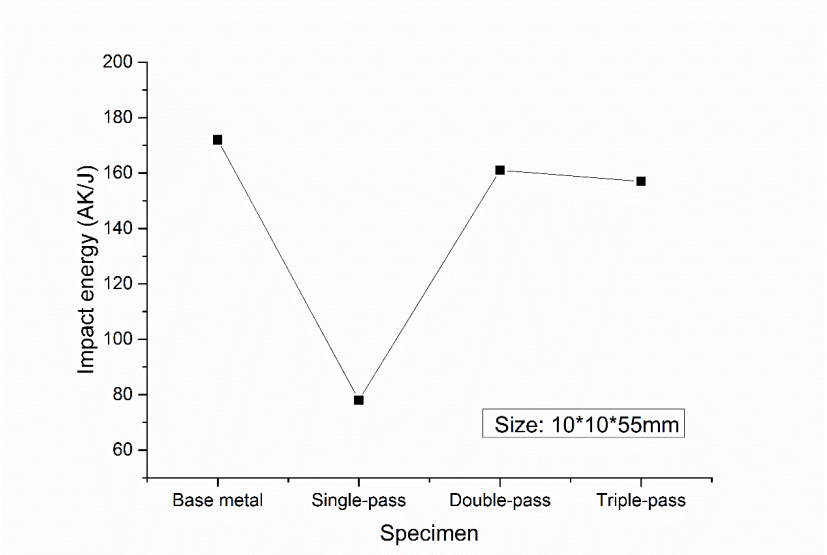

Figure 4. Impact energy of specimens 2507 base metal and after different thermal cycle.

Fig. 4 showed the relationship between welding pass and absorbing impact energy. The absorbing impact energy of base metal was 172 AK/J. As the welding pass grew from 1 to 3, the values firstly decreased and then increased. It was widely known that the impact toughness and tensile strength of ferrite were not good while austenite had satisfactory ductility and toughness. As discussed above, the specimen after first-pass thermal cycle suffered the ferritization. So that the decrease of austenite led to the degradation of impact toughness. But when the second and third pass welding were performed, the reappeared austenite increased the impact toughness.

3.3. Pitting resistance

Fig. 5 was the typical curves of thermal simulated specimens in CPT test, in which the current density kept steady at a small value of about 1×10^{-6} A/cm^{-2} during the initial heating, and then abruptly rose as the stable pitting occurred. The results of repeated CPT measurements and the average values were listed in Table 3, indicating the excellent reliability of this method.

After the first-pass thermal cycle, the CPT of specimens decreased from 84.2 °C to 69.9 °C, once more confirmed it's deteriorated microstructure. While the second and third pass welding was performed, the CPT of specimens slightly increased to 73.1°C and 72.7°C, demonstrating the similar restoration effect. Besides, previous research suggested that the geometrical feature of the electrode

surface could influence the current density distribution during the chemical reactions [30,31], which may also affect the corrosion rate.

Table 3. Repeated CPT measurements and the average values of different specimens.

Specimens	No.1 (°C)	No.2 (°C)	No.3 (°C)	Aver. (°C)
Base metal	84.9	83.4	84.3	84.2
Single-pass	69.3	70.9	69.5	69.9
Double-pass	73.9	72.8	72.6	73.1
Triple-pass	72.5	72.5	73.1	72.7

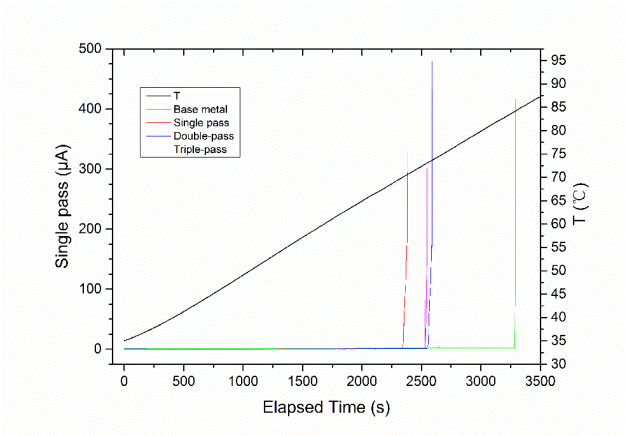

Figure 5. Typical curves of critical pitting temperature. Electrolyte: 1.0 M NaCl; applied potential: 750mV (SCE); temperature increasing rate: 1°C/min.

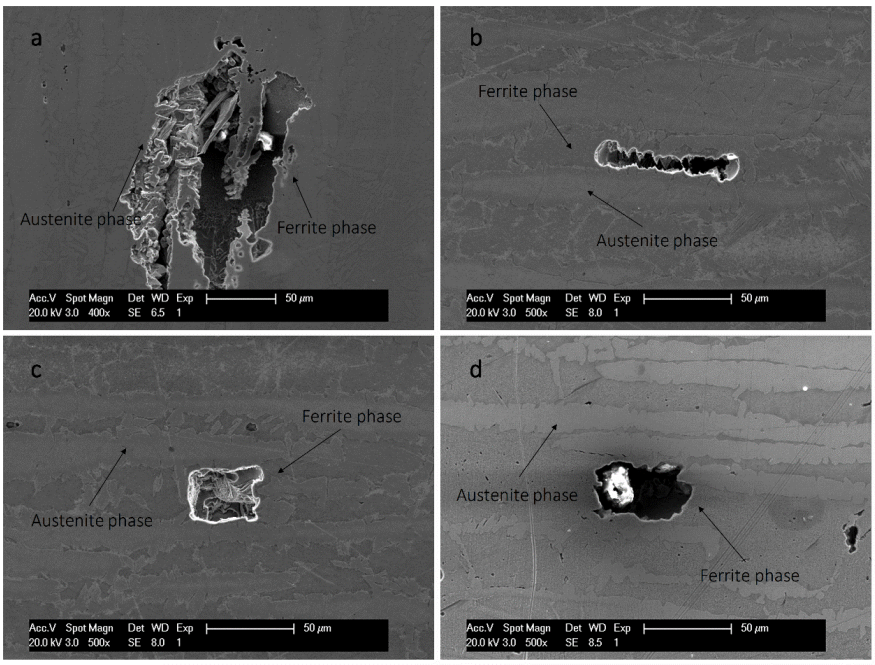

Figure 6. Pit morphologies of DSS 2507 after CPT measurements. a. base metal; b. single-pass HAZ; c. double-pass HAZ; d. triple-pass HAZ.

The morphologies of stable pitting in 2507 base metal and multi-pass welded HAZ were shown in Fig. 6. It could be observed that pitting of base metal occurred in ferrite-austenite area, while in first-pass, second-pass and third-pass welded HAZ pits were all located in ferrite phase. It suggested that the ferrite to be weaker phase after welding.

3.4. Relationship between pitting resistance and microstructure evolution

In duplex stainless steels, different pass of welding thermal cycle could lead to the evolution of microstructure, viz. the variation of ferrite/austenite ratio. A different phase ratio would result in a different distribution of alloy elements in the two phases and then change the corrosion resistance of ferrite and austenite respectively. For duplex stainless steels, Cr and Mo concentrated in ferrite, whereas Ni and N concentrated in austenite. Therefore, in the base metal, differences of alloy element contents between the two phases were the largest. But thanks to the approximately equivalent PREN value of the two phases, the corrosion resistance of ferrite and austenite tended to be equal. After suffering the first-pass welding, the amount of ferrite increased so that the corresponding mass fraction of Cr and Mo in ferrite decreased, which brought about a relatively lower PREN value of ferrite and finally degraded its corrosion resistance. In the subsequent welding pass, especially the second one, the DSS underwent a thermal cycle similar to solid solution treatment, during which austenite reformed. At the same time, Cr and Mo re-diffused into ferrite, enhancing its PREN value and improving its pitting resistance. However, different from lower alloyed DSS 2304, the high content of Ni and N in 2507 stabilized austenite during the welding process. So the ferritization and restoration effect in 2507 was not as evident as that in 2304. Besides, although the follow-up welding thermal cycle could amend the microstructure of 2507 to some extent, the pitting still occurred in ferrite, indicating that multi-pass welding could not totally restore the corrosion resistance of ferrite.

Recently, many authors reported their investigations in this field. Salvador *et al.* [32] studied the FCAW repair cycles in DSS2304 and drew the conclusion that the corrosion resistance was depressed as the number of repair cycles increased. Geng *et al.* [33] concentrated on GTA-welding joint in DSS2205 and found that a great deal of secondary austenite appeared during the second pass. Eghlimi *et al.* [34] compared the phase composition and microstructure of DSS2507 as a cladding material in GTA-welding. The results showed that thermally-activated secondary austenite did not influence the corrosion behavior significantly. Chehuan *et al.* [35] focused on GMA-welding with different heat inputs and claimed that the simple presence of secondary austenite did not necessarily decrease the corrosion resistance. In agreement with the works mentioned above, we also found the precipitation of secondary phases and microstructure transformation in DSS2507 after thermal simulation. But there were some new findings about the influence of precipitation in the present work. As a high-alloyed stainless steel, 2507 tends to form more intermetallic phases, which requires further research to clarify.

4. CONCLUSION

In multi-pass welding, the microstructure of DSS 2507 was impaired by the first-pass thermal cycle, and the toughness and corrosion resistance of the specimen was degraded by the redistribution of alloy elements in austenite and ferrite. To some extent, the follow-up thermal cycle, which was similar to a solid solution treatment, could amend the microstructure of HAZ and improve its pitting resistance. Besides, the third-pass welding had little influence on the corrosion property of DSS 2507.

ACKNOWLEDGEMENTS
The author are grateful to Gang Hu for his great help with SEM characterization and would like to acknowledge the helpful collaboration of Baosteel. This work is financially supported by the National Science Foundation of China (Grant Nos. 51371053, 51131008 and 51501041).

References

1. C. J, B. S, in: Proc. Conf Duplex Stainless Steels, 1991, pp. 3-38.
2. J.O. Nilsson, *Mater. Sci. Technol.*, 8 (1992) 685-700.
3. T. Ogawa, T. Koseki, Weld J, 68 (1989) S181-S191.
4. V. Muthupandi, P.B. Srinivasan, V. Shankar, S.K. Seshadri, S. Sundaresan, *Materials Letters,* 59 (2005) 2305-2309.
5. Y. Li, J. Liu, Y. Deng, X. Han, W. Hu, C. Zhong, *Journal of Alloys and Compounds*, 673 (2016) 28-37.
6. E. Capello, P. Chiarello, B. Previtali, M. Vedani, *Mater. Sci. Eng. A-Struct. Mater. Prop. Microstruct. Process*., 351 (2003) 334-343.
7. V. Muthupandi, P.B. Srinivasan, S.K. Seshadri, S. Sundaresan, *Mater. Sci. Eng. A-Struct. Mater. Prop. Microstruct. Process.,* 358 (2003) 9-16.
8. C. Zhong, F. Liu, Y.T. Wu, J.J. Le, L. Liu, M.F. He, J.C. Zhu, W.B. Hu, *Journal of Alloys and Compounds*, 520 (2012) 11-21.
9. Y. Gu, J. Liu, S. Qu, Y. Deng, X. Han, W. Hu, C. Zhong, *Journal of Alloys and Compounds*, 690 (2017) 228-238.
10. B. Deng, Y.M. Jiang, J. Gao, J. Li, *Journal of Alloys and Compounds*, 493 (2010) 461-464.
11. C.M. Garzon, A.J. Ramirez, *Acta Materialia,* 54 (2006) 3321-3331.
12. J.J. Le, L. Liu, F. Liu, Y.D. Deng, C. Zhong, W.B. Hu, *Journal of Alloys and Compounds*, 610 (2014) 173-179.
13. A.J. Ramirez, J.C. Lippold, S.D. Brandi, *Metall. Mater. Trans. A-Phys. Metall. Mater. Sci.*, 34A (2003) 1575-1597.
14. R. Badji, M. Bouabdallah, B. Bacroix, C. Kahloun, K. Bettahar, N. Kherrouba, *Mater. Sci. Eng. A-Struct. Mater. Prop. Microstruct. Process.,* 496 (2008) 447-454.
15. M.J. Huh, S.B. Kim, K.W. Paik, Y.G. Kim, *Scr. Mater.,* 36 (1997) 775-781.
16. T.H. Chen, J.R. Yang, *Mater. Sci. Eng. A-Struct. Mater. Prop. Microstruct. Process.,* 338 (2002) 166-181.
17. H.Y. Liou, R.I. Hsieh, W.T. Tsai, *Corrosion Science,* 44 (2002) 2841-2856.
18. H.Y. Liou, R.I. Hsieh, W.T. Tsai, *Materials Chemistry and Physics,* 74 (2002) 33-42.
19. T.A. Palmer, J.W. Elmer, S.S. Babu, *Mater. Sci. Eng. A-Struct. Mater. Prop. Microstruct. Process.,* 374 (2004) 307-321.
20. H. Sieurin, R. Sandstrom, *Mater. Sci. Eng. A-Struct. Mater. Prop. Microstruct. Process*., 418 (2006) 250-256.

21. H. Tan, Z.Y. Wang, Y.M. Jiang, Y.Z. Yang, B. Deng, H.M. Song, J. Li, *Corrosion Science*, 55 (2012) 368-377.
22. L.D. Chen, H. Tan, Z.Y. Wang, J. Li, Y.M. Jiang, *Corrosion Science*, 58 (2012) 168-174.
23. Y.M. Jiang, H. Tan, Z.Y. Wang, J.F. Hong, L.Z. Jiang, J. Li, *Corrosion Science*, 70 (2013) 252-259.
24. D. Rosenthal, *Transactions of the ASME*, 68 (1946) 849-866.
25. R. J. Brigham, E.W. Tozer, *Corrosion*, 29 (1973) 33-36.
26. B. Deng, Y. M. Jiang, J.X. Liao, Y.W. Hao, C. Zhong, J. Li, *Applied Surface Science*, 253 (2007) 7369-7375.
27. Macdonal.Dd, D. Owen, *J. Electrochem. Soc*., 120 (1973) 317-324.
28. H. Tan, Y.M. Jiang, B. Deng, T. Sun, J.L. Xu, J. Li, *Materials Characterization*, 60 (2009) 1049-1054.
29. L. H. Zhang, Y.M. Jiang, B. Deng, W. Zhang, J.L. Xu, J. Li, *Materials Characterization*, 60 (2009) 1522-1528.
30. J. Liu, W.B. Hu, C. Zhong, Y.F. Cheng, *Journal of Power Sources*, 223 (2013) 165-174.
31. J. Liu, B. Chen, Y. Kou, Z. Liu, X. Chen, Y. Li, Y. Deng, X. Han, W. Hu, C. Zhong, *Journal of Materials Chemistry A*, 4 (2016) 11060-11068.
32. C.F. Salvador, R.A. Antunes, *Corrosion Engineering Science and Technology*, (2016) 1-8.
33. S.N. Geng, J.S. Sun, L. Y. Guo, H.Q. Wang, *journal of manufacturing processes*, 19 (2015) 32-37.
34. A. Eghlimi, M. Shamanian, K. Raeissi, *Surface and Coatings Technology*, 244 (2014) 45-51.
35. T. Chehuan, V. Dreilich, K.S. de Assis, F.V.V. de Sousa, O.R. Mattos, *Corrosion Science*, 86 (2014) 268-274.